J Fail. Anal. and Preven.
https://doi.org/10.1007/s11668-020-01076-5

TECHNICAL ARTICLE—PEER-REVIEWED

Assessment of the Degraded High-Pressure Blades in a Land-Based Gas Turbine

Khier Sabri · Mohamed Ouali Si-Chaib · Mohamed Gaceb

Submitted: 19 February 2020 / in revised form: 23 September 2020 / Accepted: 1 November 2020

Abstract The purpose of this paper is to evaluate high-pressure turbine blades after a long-term thermal exposure in a land-based gas turbine. Emphasis is placed upon structure and composition of the various layers evolving, on the one hand, due to hot oxidation/corrosion attacks and, on the other hand, because of interdiffusion phenomena between the substrates and their protective coatings. This work therefore discusses the influence of γ'-Ni_3 (Al, Ti) precipitates coarsening, needle σ-phase nucleation, and $M_{23}C_6$-Carbides formation on the hardness properties of blades. In addition, this assessment attempts to evaluate the influence of γ'-Ni_3 (Al, Ti) orientation changes and crystallites size growth on the intrinsic degradation of GTD-111 and IN738LC substrates.

Keywords (CC) GTD-111 superalloy · (CC) IN738LC superalloy · NiPtAl coating · VPS coating · Needle σ-phase · Hot corrosion/oxidation

Introduction

Various industrial gas turbine blades made of conventionally cast (CC) GTD-111, and (CC) IN738LC nickel-based superalloys are now approaching or have reached their design lifetime [1–8]. Hence, huge attention has been paid to the blade's microstructural changes during service because of combined effects of high temperatures and stresses, which can change the whole substrate behavior and affect the life span [9, 10]. In addition, the strength of high-pressure IN738LC blades coated via Pt-modified aluminide was based on the internal variables: the FCC γ'-Ni_3 (Al, Ti) precipitates coarsening, needle σ-phase nucleation, and MC-Carbide particles degeneration in γ-matrix to form a continuous linear network of Cr-rich $M_{23}C_6$ at the grain boundaries [11–13]. Rafiee et al. [14] and El-Bagoury et al. [15] have demonstrated that interdiffusion phenomenon took place between the substrate and the NiPtAl coating leading to the formation of a fragile $\gamma/\gamma'/\sigma$ microstructure under interdiffusion zone (IDZ). In a recent paper by Golezani et al. [16], this fragile zone seriously influences the Inconel 738LC substrate hardness and mechanical properties. Moreover, $M_{23}C_6$-Carbides contribution to the grain boundary sliding could not be neglected. Previous results have documented that the outstanding creep strength of these superalloys is attributed to bimodal distribution of γ'-Ni_3 (Al, Ti) particles [17–19]. In this context, the γ'-Ni_3(Al, Ti) coarsening within equiaxed GTD-111 superalloys of creeping turbine blades were discussed by many investigators [20, 21]. Thereby, it is adequate to link the degradation of blades superalloys to the γ'-Ni_3(Al, Ti) particles growth [22, 23]. Lifschitz–Slozov–Wagner's theory is the preferred technique to determine the extent of degradation based on the mean size of γ'-Ni_3(Al, Ti) particles [24]. Mastromatteo et al. [25] and Dadkhah et al. [26] indicate that tracking the γ'-Ni_3 (Al, Ti) mean size is the key to accurately estimating the consumed creep life of blades. In-service degeneration of MC-carbide particles within γ-matrix and precipitation of $M_{23}C_6$-carbide phases along grain boundaries were discussed in the previous work [27], indicating these mechanisms worsen the degradation in blade mechanical properties. The condition of plasma spray coating in a corrosive environment

K. Sabri (✉) · M. O. Si-Chaib · M. Gaceb
Laboratory of Petroleum Equipment's Reliability and Materials, Hydrocarbons and Chemistry Faculty, Université M'Hamed Bougara de Boumerdès, UMBB, Boumerdès, Algeria
e-mail: sabrikhier@univ-boumerdes.dz

Published online: 28 January 2021

has been gaining interest from the operators in decision making about the refurbishment or returning the blades to service for another overhaul period [28, 29]. Likewise, NiPtAl diffusion coating transformation due to hot corrosion/oxidation attacks has been identified as another mechanism of importance in recent years [30]. Contemporary studies focus on the complex relationships linking the interdiffusion phenomenon and the mechanical behavior of the different IN738LC/NiPtAl strata [31]. In the literature, a variety of theories and results has been published to explain the β-(Ni, Pt) Al transformation and decomposition [32]. Caron et al. [33] and Walston et al. [34] have documented the NiPtAl coating degradation mechanisms during service at high temperature. The finding was that initial β-(Ni, Pt) Al single-phase transforms progressively into a γ'-Ni_3Al phase with the aluminum content reduction in the coating due to oxidation. Inward diffusion of (Al, Pt), and outward diffusion of Co, Cr, or Ti from substrate, tend to increase the β-phase morphology and composition changes. As reported by Narita [35], the β-phase loses its protective characteristics once changed to biphasic structure $\beta + \gamma'$. Finally, only γ-phase remains, while NiPtAl coating is fully consumed. These transformations decrease the NiPtAl coating strength thus leading to cracks initiation and propagation.

This article focuses on the transformation of NiPtAl coating due to hot corrosion and the interdiffusion with IN738LC substrate. The microstructure of degraded GTD-111 blade material with vacuum plasma spray (VPS) coating was investigated as well. The impacts of γ'-Ni_3 (Al, Ti) coarsening, needle σ-phase nucleation, and $M_{23}C_6$-carbides precipitation on blades hardness properties were analyzed and discussed. Based on the metallurgical examinations, the GTD-111 substrate shows superior

Table 1 The degraded blades history

NiPtAl/IN738LC (CC) blade	VPS coating/GTD-111 (CC) blade
800 °C	820 °C
10 MW	10 MW
48,000 h (of base load service)	48,000 h (of base load service)
7000 RPM	5100 RPM
1000 start/stop	1000 start/stop

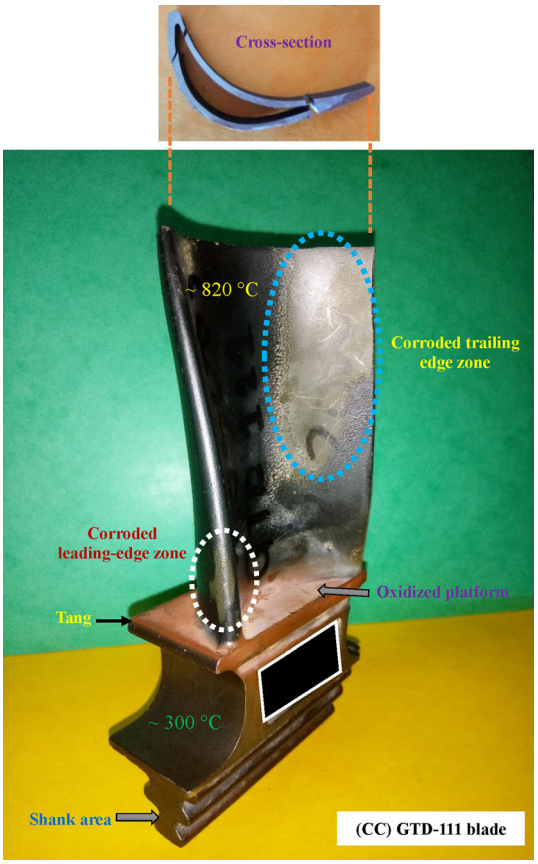

Fig. 1 Degraded GTD-111 blade

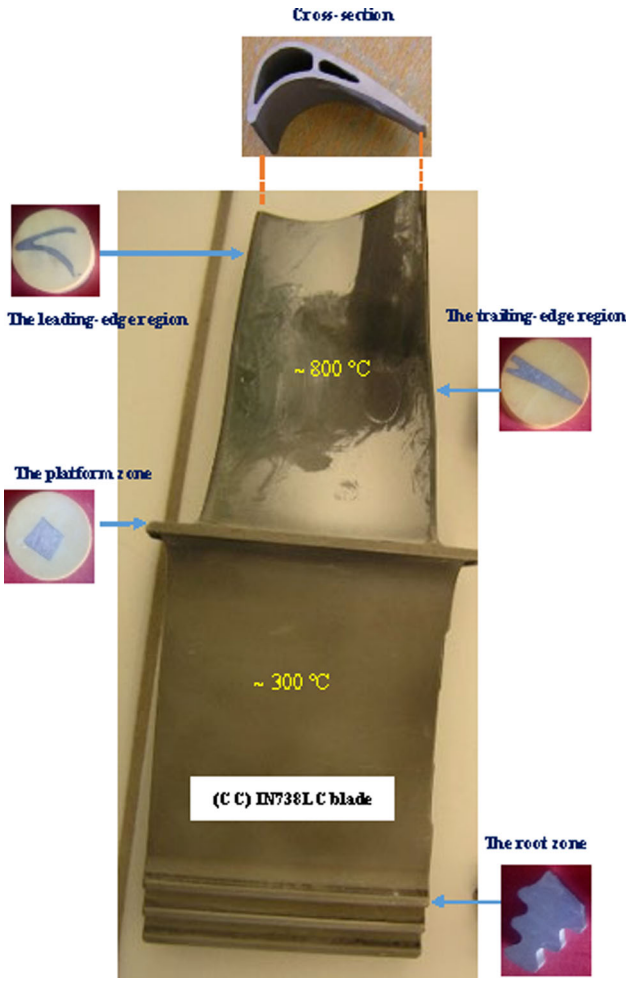

Fig. 2 Degraded IN738LC blade

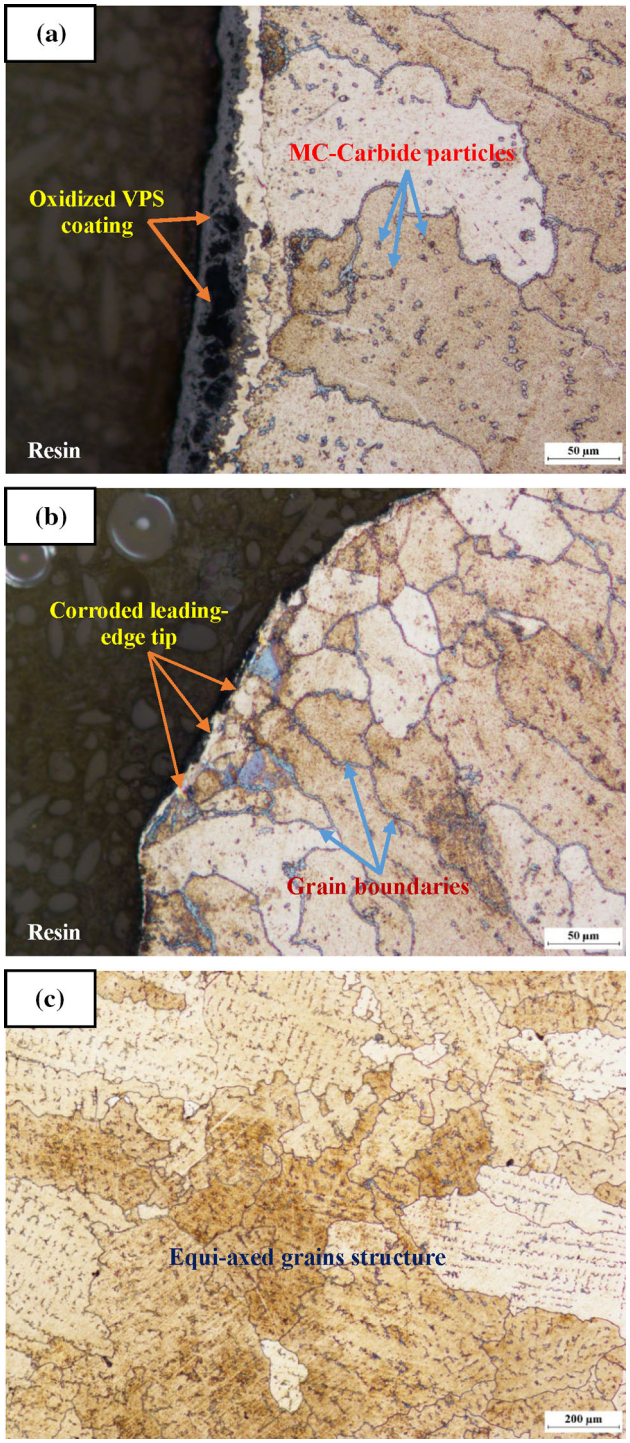

Fig. 3 Optical photomicrographs showing the grains structure of GTD-111 superalloy at the airfoil trailing-edge corroded region. (**a**) Oxidized VPS coating. (**b**) Corroded leading-edge tip. (**c**) Magnified view of grains structure

hardness properties in comparison with IN738LC substrate. This is attributed to the absence of the needle σ phase and the slow growth of γ'-$Ni_3(Al, Ti)$ precipitates. The vacuum

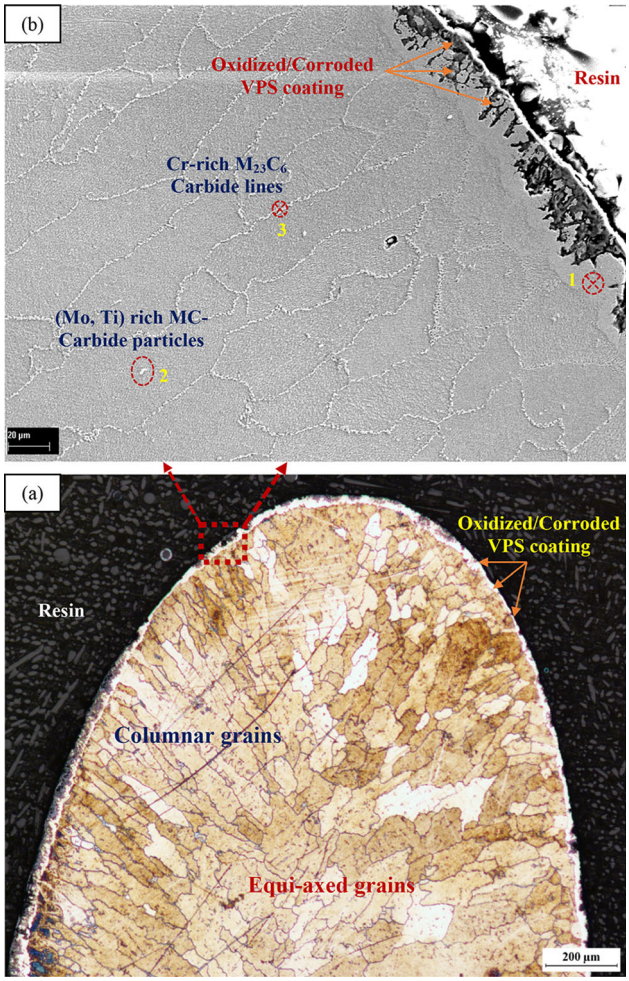

Fig. 4 Microstructure of the corroded/oxidized trailing-edge zone. (**a**) Optical photomicrograph of the trailing-edge tip. (**b**) Magnified SEM photomicrograph of the trailing-edge tip

plasma spray (VPS) coating also presents superior hot corrosion resistance compared to the NiPtAl coating.

Preparatory Procedures

Turbine Blades Operating History

The turbine blades operational history is shown in Table 1. Using a PRESI MECATOME T300 machine a variety of samples were sectioned from the leading-edge and trailing edge of degraded turbine blades. The less degraded areas (shank) were examined to establish a pre-service microstructure/material benchmark. After samples mounting, surface polishing, and ultrasonic cleaning, the IN738LC/NiPtAl samples were etched with a Murakami's reagent of the following composition: 10 g $K_3Fe(CN)_6$, 10 g KOH, and 100 mL water, mixed fresh then heated for few seconds at 80 °C. In parallel, the VPS/GTD-111

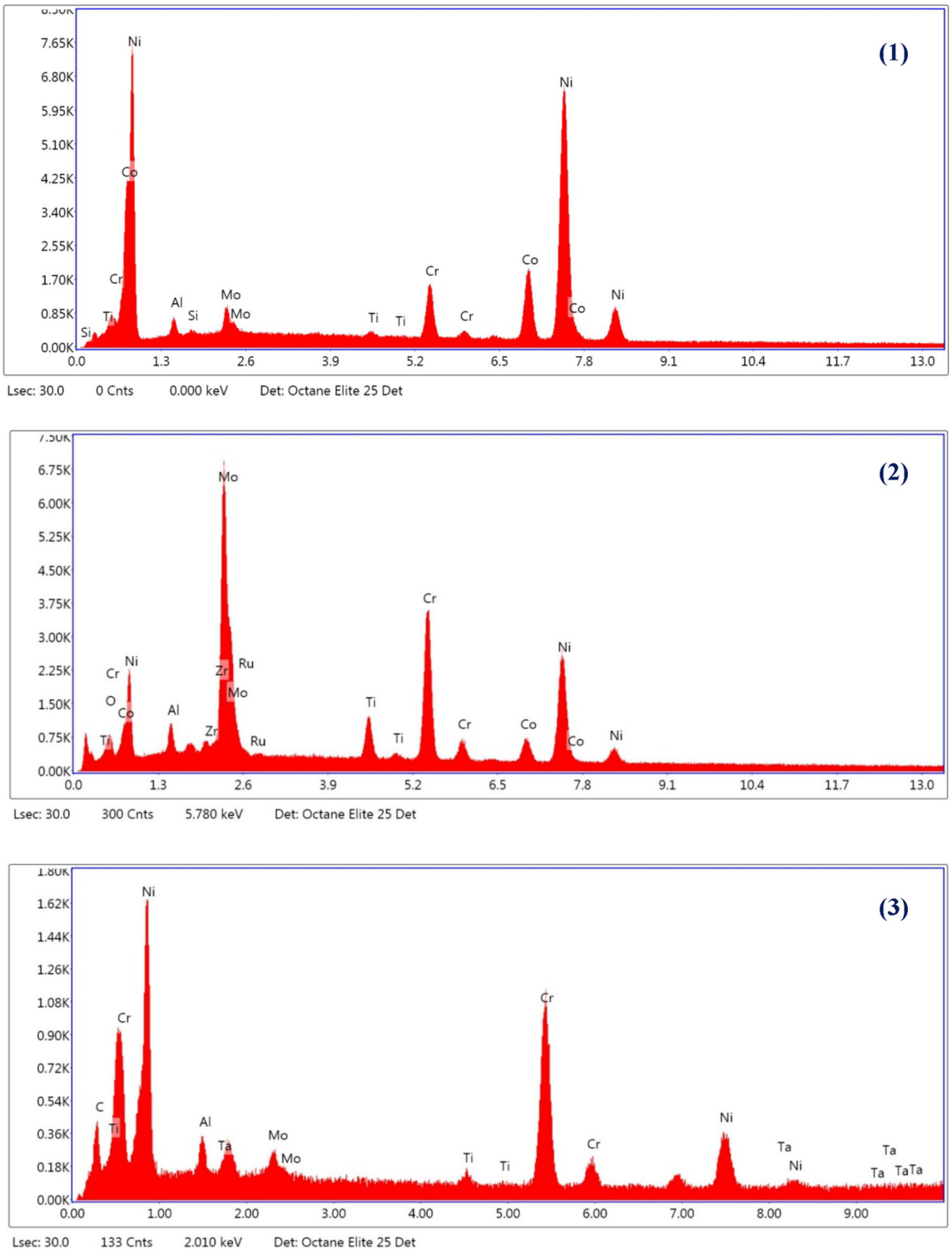

Fig. 5 Representative EDS spectra illustrating the elementary composition of: (1) the non-oxidized VPS coating. (2) The MC-carbide particles. (3) The $M_{23}C_6$ carbides

samples were immersed in a Marble's reagent of the following composition: 10 g $CuSO_4$, 50 ml HCL, and 50 ml H_2O.

Optical Microscopy

Prepared (etched) surfaces of the samples initially were analyzed by means of NIKON ECLIPSE LV100ND optical

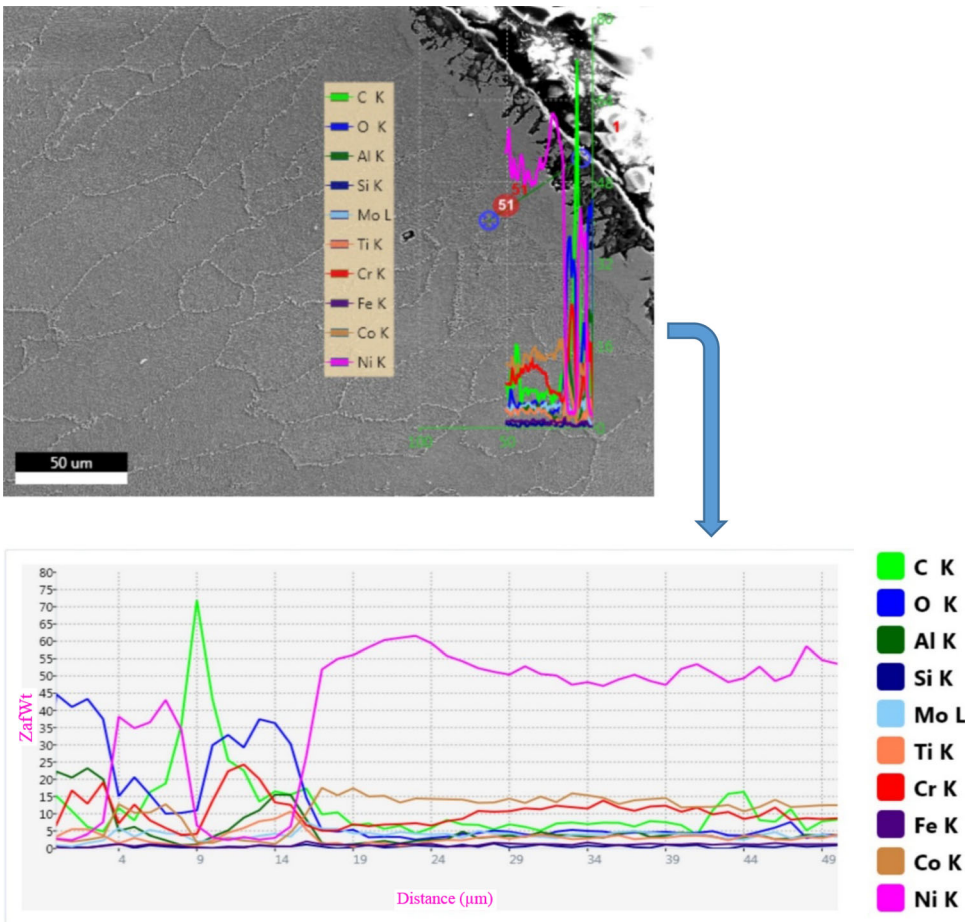

Fig. 6 Line profiles taken on VPS/GTD-111 strata of the oxidized trailing-edge region

microscope to observe on the one hand, the grains pattern, on the other hand, the coatings corrosion/oxidation extent.

Electron Microscopy

Characterizing and identifying the chemical composition of the blade strata was achieved using a ZEISS Gemini SEM-300 coupled with energy-dispersive x-ray spectroscopy.

The γ' Precipitates Mean Size

To evaluate the thermally degraded blade zones, the mean size and volume fraction of γ'-Ni_3 (Al, Ti) precipitates were quantified using ImageJ software.

Micro-hardness Tests

The micro-hardness tests were performed on the prepared surfaces at room temperature using a BUEHLER WILSON VH3300 Tester, under 3 N loads with a vickers indenter.

XRD Analysis

BRUKER D8DISCOVER x-ray diffractometer was utilized to identify the major phases within IN738LC blade. The source generated incident CuKa x-rays having a wavelength $\lambda = 1.5418$ A°. The diffraction patterns were detected over the 2θ range from 2 0° to 100°, with a scanning rate of 1°/min. XRD patterns were plotted and analyzed using OriginLab and High Score Plus software.

Results

Visual Inspection

The degraded blades exhibit a hollow interior as shown in Figs. 1 and 2. In the as-received condition, the (CC) GTD-111 blade displayed severe hot corrosion attacks at the airfoil hot section (blue and white circles). Furthermore, the airfoil region is black in color with a bit of brownish-red color. The shank zone did not show any discoloration or deformation (unaffected). The blade coating was corroded and stripped off the airfoil in some areas due to the

combined hot corrosion/erosion effects. The (CC) IN738LC blade presented in Fig. 2 also displays the presence of dark-brown color at the airfoil hot section. The shank zone was free of degradation.

Characterization of GTD-111 Blade

The corroded/oxidized trailing-edge zone (blue circle) shown in Fig. 1 was at first inspected using optical microscopy. The optical photomicrographs in Fig. 3 exhibit the conventionally cast (CC) structure of the GTD-111 nickel-based superalloy with its oxidized vacuum plasma spray (VPS) coating. The VPS coating deposited on GTD-111 substrate had sustained a severe hot corrosion in operation, as shown in Fig. 3a. Even worse, the corroded VPS coating had stripped off at the trailing-edge tip. Figure 3b shows the presence of a variety of MC-carbide particles in interior grain, and $M_{23}C_6$-carbide lines at grain boundaries. According to Fig. 3c, the grains mean size in this degraded region is around $\sim$ 120 µm. Figure 4a shows the conventionally cast structure of the corroded trailing-edge zone. In this cast, GTD-111 substrate two-grain structures were developed: columnar grains at the mold walls, and equiaxed grains at the center. As presented in Fig. 4b, the degraded trailing-edge microstructure reveals the presence of Cr-rich $M_{23}C_6$-lines network at grain boundaries and elongated/globular MC-carbides within the grains. Additionally, the VPS coating had endured a high level of corrosion/oxidation attacks. Figure 5 displays the representative EDS spectra performed at the points 1, 2, and 3 mentioned in Fig. 4b. According to EDS spectrum (1), the non-oxidized VPS layer was found to have the following composition: 72.97Ni 16.08Co 5.9Cr 2.88Mo 1.77Al 0.24Si 0.16Ti (wt.%). Based on the spectrum (2), the MC-carbide particles precipitated within GTD-111 grains interior are rich in Mo, and Ti elements. EDS spectrum (3) confirms the precipitation of Cr-rich $M_{23}C_6$-lines network at the grain boundaries of the degraded GTD-111 substrate. In addition, the EDS line scan results presented in Fig. 6 confirm the outward diffusion of (Al, Cr) coating elements due to high-temperature oxidation. The latter explains the formation of $(Cr, Al)_2O_3$ oxide scales. Small traces of Ti, Mo, Fe, and Co oxides were generated in the outer surface. At the non-oxidized zones of VPS coating, the element concentrations return to their near steady state.

Moreover, the microstructure of the oxidized leading-edge zone is presented in the SEM micrographs of Fig. 7. This degraded region also contains a variety of MC-carbide particles and continuous lines network of Cr-rich $M_{23}C_6$-carbides, as shown in Fig. 7a. According to Fig. 7b, the VPS coating of the leading-edge corroded/eroded zone was stripped off (the white circle shown in Fig. 1). However, there is a diffusion band at the outer surface of GTD-111 substrate containing blocky Al_2O_3 oxides. The EDS line scan results presented in Fig. 8 show the stability in elements concentrations across the strata (non-oxidized VPS coating/GTD-111 substrate).

The main phenomenon occurring in the degraded blades is the coarsening and coalescence of γ'-Ni_3 (Al, Ti) precipitates, as shown in Fig. 9. The FCC γ' (Ni_3, Al) mean size in the collected images is measured using ImageJ software, as given in Table 2. The newly introduced degradation index is based on the γ' precipitates mean size according to the following expression:

$$D_i = \frac{\gamma'_t}{\gamma'_t} \qquad \text{(Eq 1)}$$

γ'_t: aged gamma prime mean size. γ'_0: initial gamma prime mean size.

From SEM micrographs (Fig. 9), the γ' precipitates had changed from a triangular form in the shank zone to completely rounded shape in the corroded trailing, leading-edge regions. This evolution reduces the creep resistance of (CC) GTD-111 blade. The hardness mean values, shown in

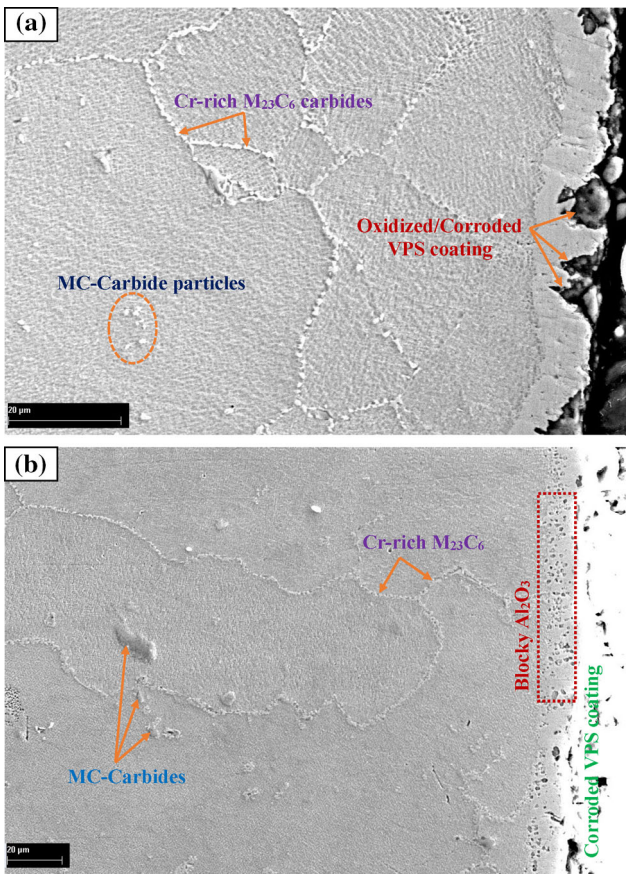

Fig. 7 SEM photomicrographs. (**a**) Microstructure of the oxidized leading-edge region. (**b**) Microstructure of the leading-edge eroded zone

Table 3, are in agreement with the γ' particles mean size in the different zones of degraded blade.

Characterization of IN738LC Blade

As shown in Fig. 10a, the leading-edge region strata (NiPtAl + IN738LC) shows a significant degradation in the substrate microstructure, and the formation of Al_2O_3 oxide scale and corrosion pits at the outer surface of coating. The β-(Ni, Pt)Al backbone layer of around $\sim$ 45 µm provides the reservoir surface of elements that will form a very protective oxide layer. A mixture of (Ti, Ta)Nb carbides, TaW particles, and (Ni, Co)Cr-rich elongated phases were precipitated in the interdiffusion zone of $\sim$ 39 µm thickness. The presence of the needle σ phase rich in (Ni, Co) Cr-W beneath the interdiffusion zone makes the IN738LC brittle during operation at 980 °C and reduces the blade creep resistance. The presence of continuous lines of Cr-rich $M_{23}C_6$ carbides at the grain boundaries was a result of the blocky MC-carbides (rich in Ta, Ti, and Nb) degeneration within the austenitic γ-matrix. These lines of $M_{23}C_6$ have an impact on the IN738LC substrate hardness properties. Based on Fig. 10b, the blade trailing-edge zone displays a complete change of the β single phase into a $\gamma + \gamma'$ microstructure. This is the best moment for coating restitution (stripping and recoat). Several cracks initiated and propagated through the consumed β layer (changed to $\gamma + \gamma'$) and the interdiffusion zone. In addition, the IN738LC substrate under the interdiffusion zone was transformed into a fragile $\sigma + \gamma + \gamma'$ microstructure. The spectrum (1) of Fig. 11 indicates that the elongated nodules in the interdiffusion zone (Fig. 10b), are rich in Cr and Co elements. The spectrum (2) performed on the precipitated needle σ phase under the interdiffusion zone (Fig. 10b) shows high concentrations in (Ni, Co) Cr-W elements. According to spectrum (3) of Fig. 11, the white particles designated by (1) in Fig. 10b are rich in Ti, Ta, and Nb.

The continuous oxidation of β-layer promotes the interdiffusion of various elements between the aluminide coating and (CC) IN738LC substrate as shown in Fig. 12a. This leads to the occurrence of γ' phase within the fragile β layer because it depends on the Al, Pt contents. Several cracks initiated in the $\beta + \gamma'$ layer, may propagate by thermal-fatigue into the IN738LC substrate. Addition of Zr has a significant effect on oxidation behavior of the Pt-

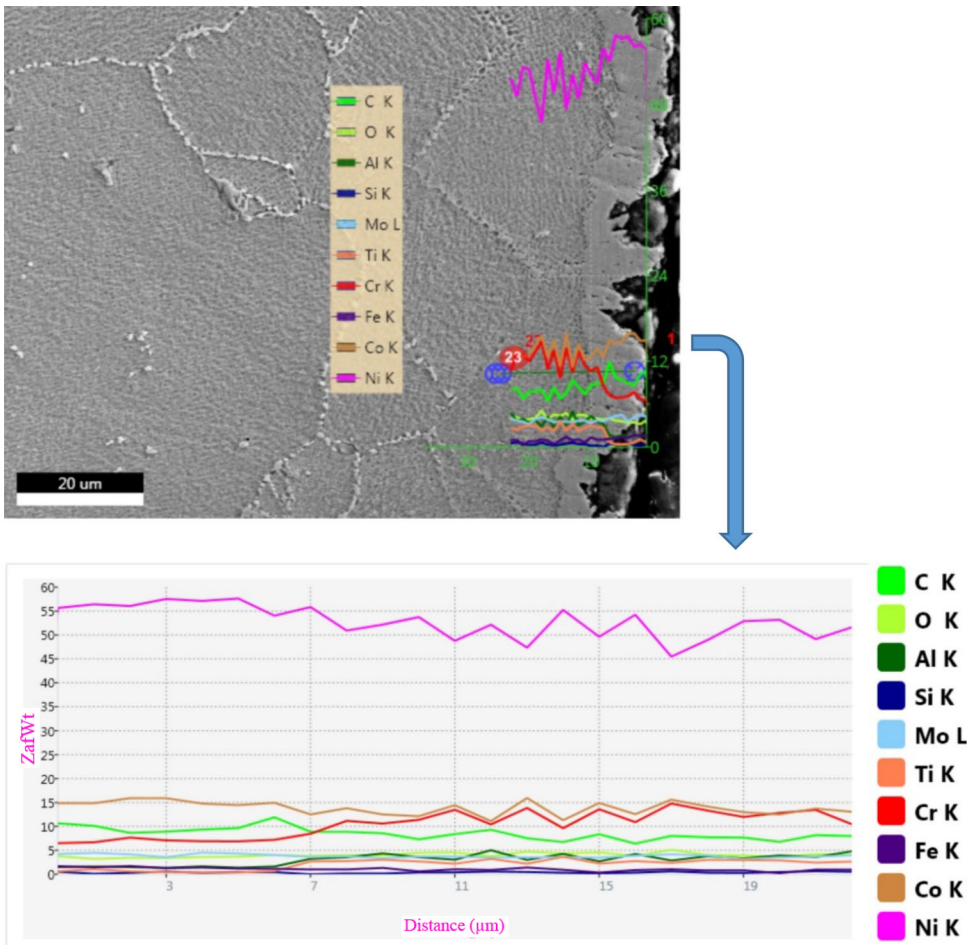

Fig. 8 Line profiles taken on VPS/GTD-111 strata of the oxidized leading-edge region

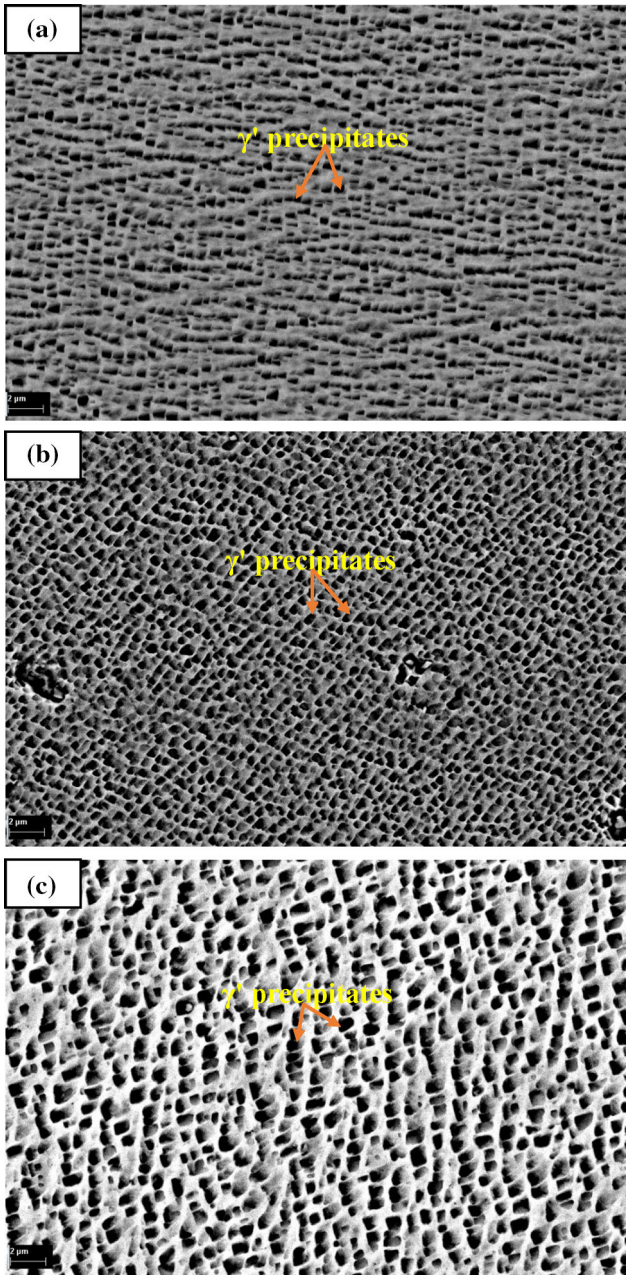

Fig. 9 SEM micrographs showing the $\gamma + \gamma'$ microstructure in the different GTD-111 blade regions, (**a**) the shank, (**b**) the leading edge, (**c**) the trailing edge

modified Ni–Al coating. The Pt also increases the activity of Al in the coating to generate an adherent Al_2O_3 scale on the outer surface. The presence of (Zr, Pt) elements in this NiPtAl coating (point 1 in Fig. 12a) is confirmed by the EDS spectrum in Fig. 13. Additionally, precipitates of C_3Al_4, and C_3Cr were observed in the interdiffusion zone. Beneath the interdiffusion zone a denuded band rich in Cr, and Co was formed. Microstructure of the IN738LC substrate presented in Fig. 12b exhibits an equiaxed grain structure. However, the presence of smooth and tortuous

Table 2 Mean size of the γ' precipitates

	Root zone		Leading-edge		Trailing edge	
Turbine blades	GTD-111	IN738LC	GTD-111	IN738LC	GTD-111	IN738LC
γ' average size (μm)	0.40	0.52	0.72	0.84	0.98	1.11
% area	39.8	34.22	45.48	37.47	47	39.71
$D_i = A_i\ (\gamma')/A_0\ (\gamma')$	1	1	1.8	1.6	2.45	2.13

Table 3 Results of the micro-hardness tests

	Root zone		Leading-edge		Trailing edge	
Turbine blades	GTD-111	IN738LC	GTD-111	IN738LC	GTD-111	IN738LC
Hardness average value (Hv)	420	430	467	563	491	619

grain boundaries inhibit the grain boundaries sliding deformation mechanism during service at ~ 980 °C. Examination of the internal cooling channel wall revealed the stripping of the external β-(Ni, Pt) Al layer as shown in Fig. 14a. Several carbide nodules mixed with a needle σ phase rich in (Cr, Co) W were also observed within IN738LC substrate. Form Fig. 14b, the presence of a thick oxide scales and micro-voids can be seen at the coating outer surface. Based on EDS spectrum shown in Fig. 15, the oxidized β-layer (point 1) is mainly composed of (Al, Cr)$_2$ O_3, Fe_2O_3 oxides. Various C_3Al_4 precipitates were also generated in this degraded β-layer. A zone of around 45 μm containing the σ-phase was generated beneath the interdiffusion zone. A variety of MC-carbide particles were found in the austenitic γ matrix of the shank, as shown in Fig. 16a. Based on EDS spectrum (1) shown in Fig. 17, these particles are rich in Ti, Ta, and Nb. In parallel, SEM micrographs of the airfoil hot section (Fig. 16b) show the presence of a network $M_{23}C_6$-carbide lines at the grain boundaries. These Cr-rich carbides are identified based on EDS spectrum (2) displayed in Fig. 17. According to Fig. 18a, the non-affected shank region reveals two kinds of FCC γ'-(Ni_3, Al) precipitates: the secondary γ' precipitates with a mean size of 0.52 μm and a 34.22% volume fraction and the tertiary γ' precipitates with a mean size of 0.1 μm. In airfoil leading-edge region, the secondary γ' precipitates with an oval shape have a 0.84 μm mean size and a 37.47% volume fraction, as shown in Fig. 18b. The mean size of the tertiary γ' particles is 0.2 μm. Figure 18c shows that trailing-edge microstructure is for the most part an irregular and coarse γ' (Ni_3, Al) particles of 1.11 μm mean size and 39.71% volume occupation. The tertiary γ'

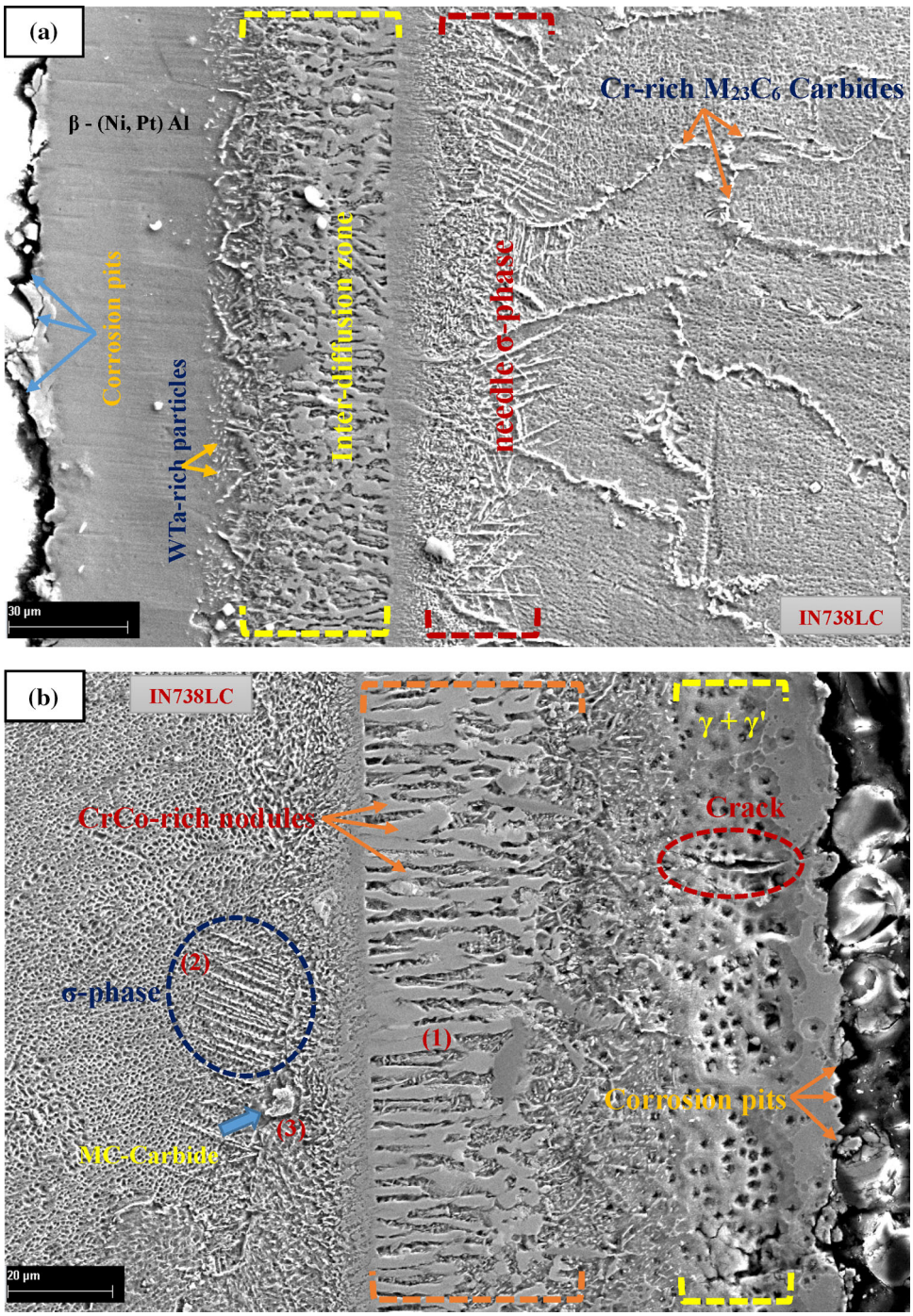

Fig. 10 SEM Micrographs illustrating the morphology of IN738LC/NiPtAl strata, (**a**) in the leading-edge zone, (**b**) in the trailing-edge zone

precipitates of 0.2 μm mean size were dispersed among the large secondary γ' particles in the grain interior. Values of the mean size of γ' (Ni_3, Al) precipitates at different regions of the degraded turbine blades are summarized in Table 2. The hardness values outlined in Table 3 provides evidence of a significant degradation in the blade airfoil region in comparison to that of the uncoated shank with an acceptable hardness value of 430 (Hv). As reported by Shejale et al. [13], tensile test results at the room temperature performed on specimens cut from the shank zone were found adequate for the IN738LC blade with yield stress = 788 N/mm^2, ultimate tensile strength = 852 N/mm^2, and the elongation equal to 4.80%. The XRD results shown in Fig. 19, indicated the presence of γ'-Ni_3 (Al, Ti) phases and $C_5NbTa_2Ti_2$ particles in the shank area. The precipitation of $M_{23}C_6$ carbides in the degraded airfoil region was clearly identified from the diffraction peaks. These $M_{23}C_6$-carbides were generated during operation

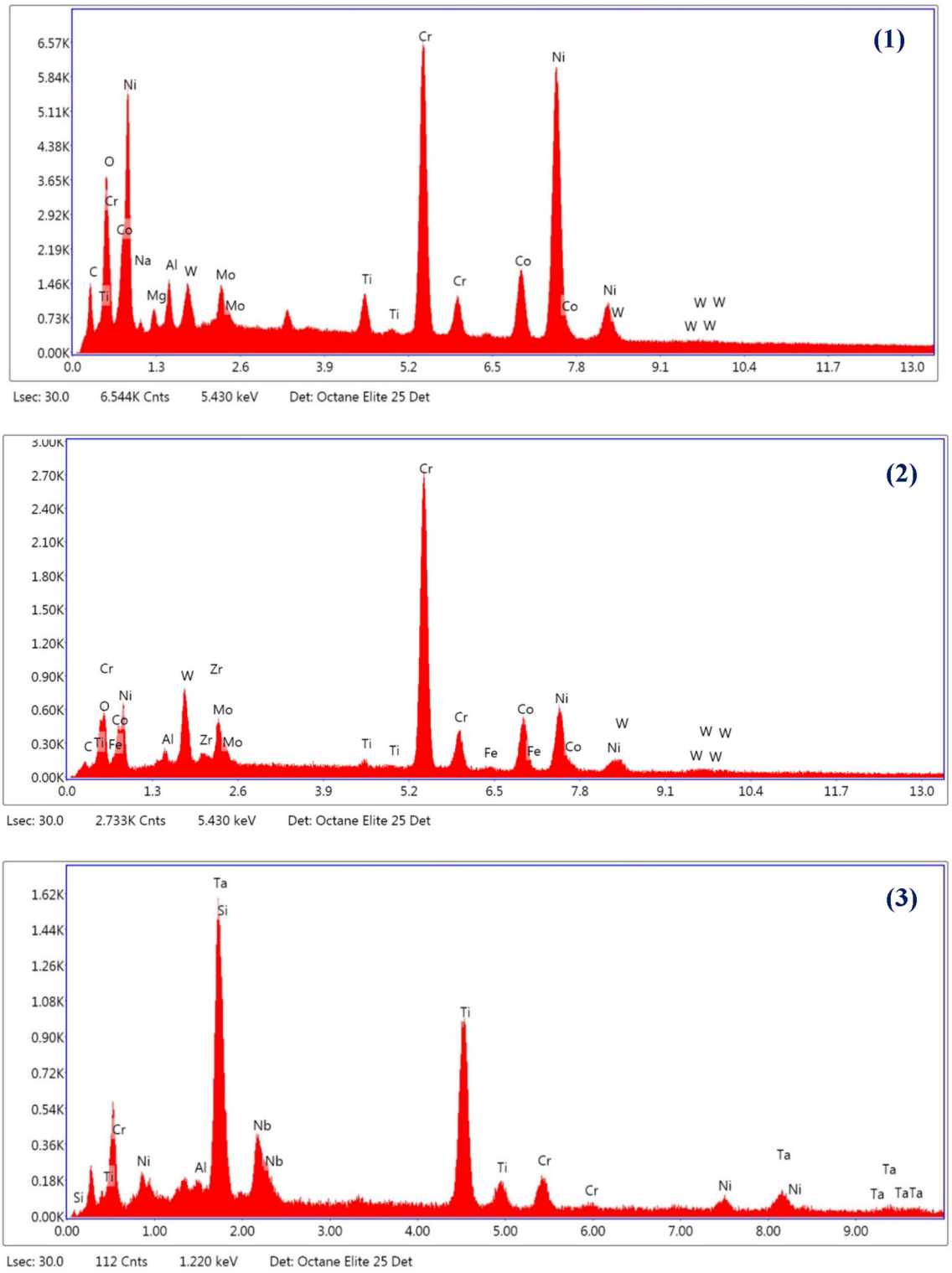

Fig. 11 EDS spectra, (1) of the CrCo-rich nodules, (2) of the σ phase, (3) of the (Ti, Ta)Nb rich carbide particles

according to the following reaction: $C_5NbTa_2Ti_2 + \gamma \rightarrow Ni_3$ (Al, Ti) + $M_{23}C_6$. The orientation of the γ'-Ni_3(Al, Ti) precipitates in the degraded airfoil section were changed in comparison to their orientation in the shank. The mean size of the γ' crystallites was calculated from the XRD data using the Scherrer equation shown below:

$$D = K\lambda/(d\cos\theta) \quad \text{(Eq 2)}$$

where D is the crystallite size (nm), K 0.9 (Scherrer constant), λ 1.54060 for CuKa l, d is the FWHM (Full Width at Half Maximum) and θ is the peak position (radians).

The mean size of γ' crystallites varied from the 20.45 nm in the shank to 39.45 nm in the airfoil. Consequently, the growth and orientation changes of γ' crystallites are considered as indicators of the plastic deformation (intrinsic strain).

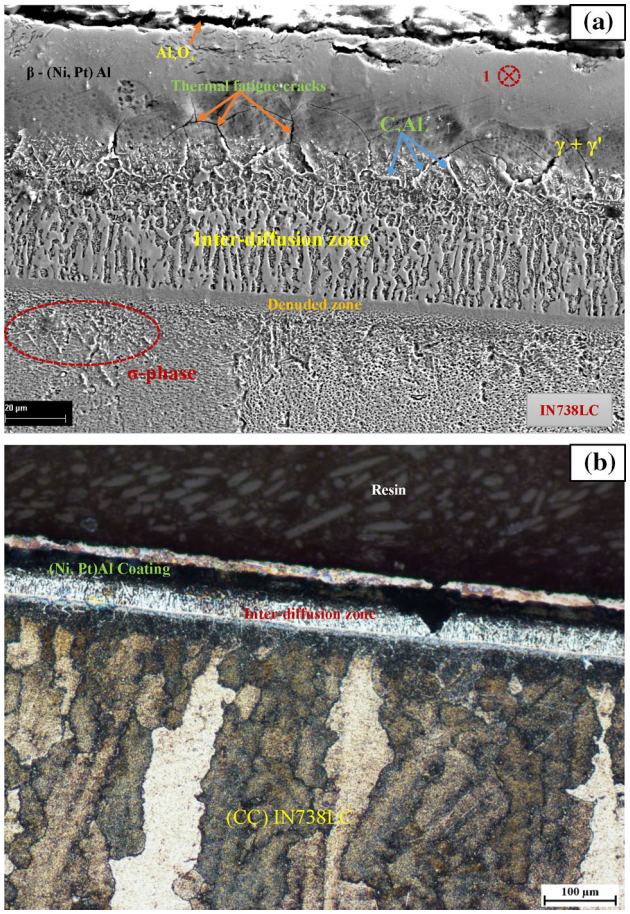

Fig. 12 Microstructure of the blade platform. (**a**) SEM micrograph of NiPtAl/IN738LC strata. (**b**) Optical micrograph of NiPtAl/IN738LC strata

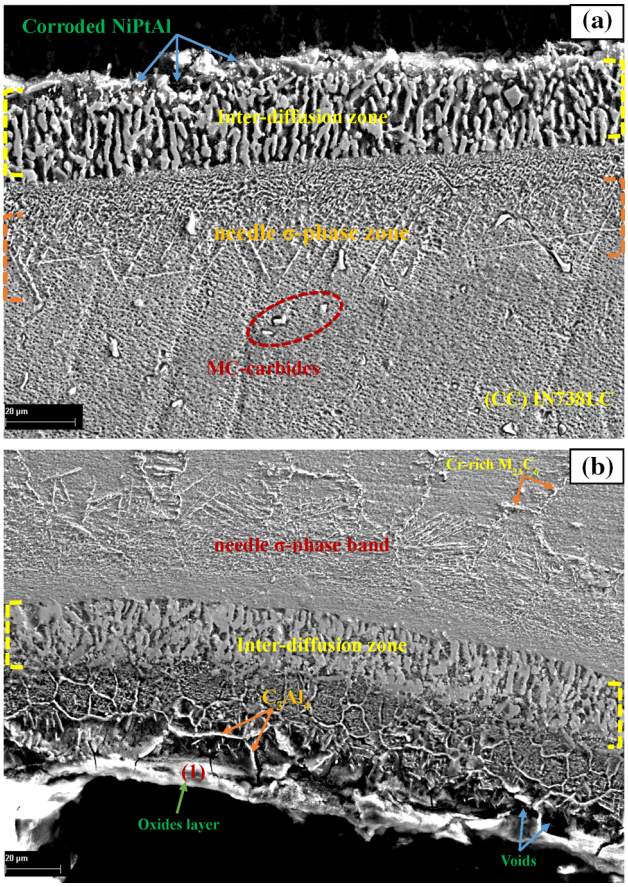

Fig. 14 SEM micrographs of the cooling channel internal wall. (**a**) Stripping of β-layer. (**b**) Micro-voids formation within β-layer

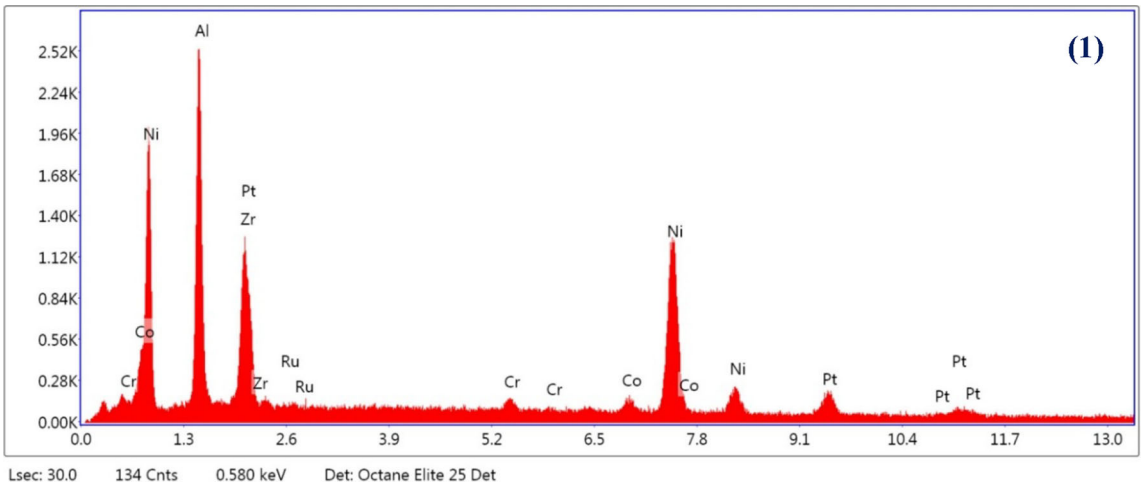

Fig. 13 EDS spectrum of the degraded β-layer

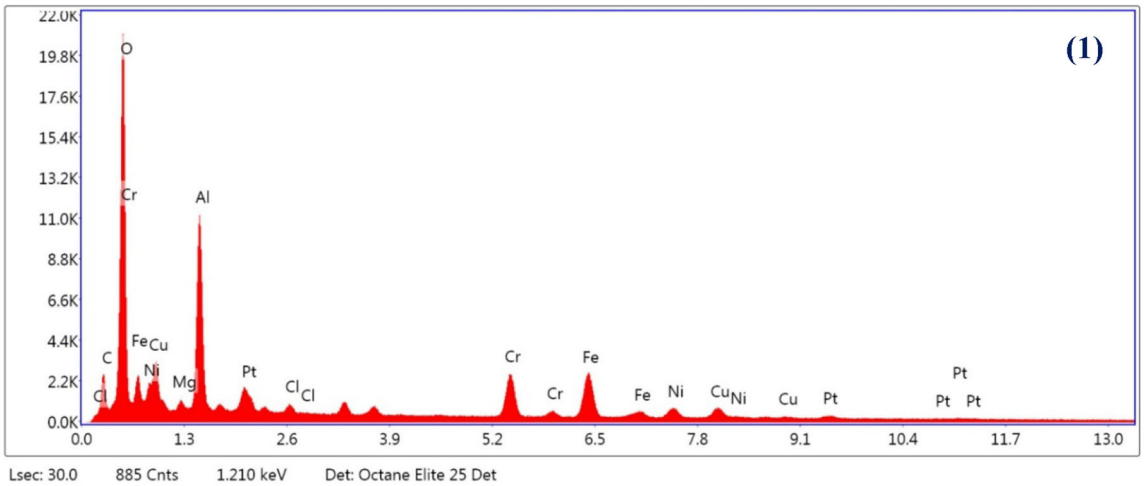

Fig. 15 EDS spectrum of the oxidized β-layer

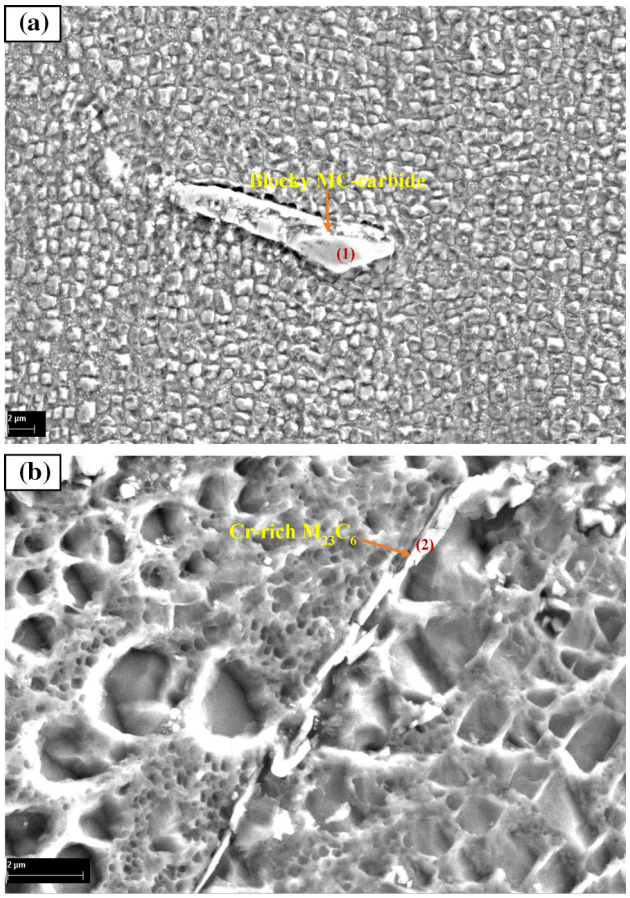

Fig. 16 SEM micrographs, (**a**) of the (Ti, Ta) Nb carbide particles in the shank, (**b**) of the $M_{23}C_6$ lines in the airfoil hot section

Discussions

The visual examination of GTD-111 blade shows the presence of a black color at the airfoil section, as shown in Fig. 1. This color is attributed to the VPS coating oxidation during operation at 820 °C. The presence of red deposits in the platform region is thought to be a result of ingestion of the mineral debris (dust, sand, and ash) contained in the hot gases arriving to the gas turbine. The severe corrosion attacks that took place at the airfoil (the blue and white circle) was a result of the alkali metal contaminants (such as Na_2So_4) deposition at the outer surface. The thermally unaffected shank zone ($\sim$ 300 °C) remains sound. However, the stage 1 blade shown in Fig. 2 revealed a dark-brown color at the airfoil section. This is a sign of the high-temperature oxidation of NiPtAl protective coating at 800 °C. The shank is unaffected (less than 300 °C).

Evaluation of the VPS/GTD-111 strata

It is clear from the optical micrographs of Fig. 3 that the microstructure of the corroded trailing-edge zone strata has evolved. The dark band at the outer surface of the VPS coating shown in Fig. 3a is attributed to the severe oxidation at 820 °C. In general, VPS coatings have good resistance to cracking and provide good refurbishment capability for the aged blade. The VPS coating at the trailing-edge tip was stripped off due to hot corrosion attacks, as shown in Fig. 3b. In addition, the equiaxed grains structure shown in Fig. 3c is a characteristic of the GTD-111 nickel-based superalloy. This grains morphology did not display any abnormality. From Fig. 4a, the small equiaxed grains generated at the outer surface of the GTD-111 substrate were a consequence of the rapid cooling near the wall at room temperature. These equiaxed grains grow in the reverse orientation to the heat flow out through the mold (columnar grains are present in the area with less undercooling). An intrinsic degradation was observed in the VPS/GTD-111 strata of the trailing-edge zone as shown in Fig. 4b. According to the EDS spectrum (1) of Fig. 5,

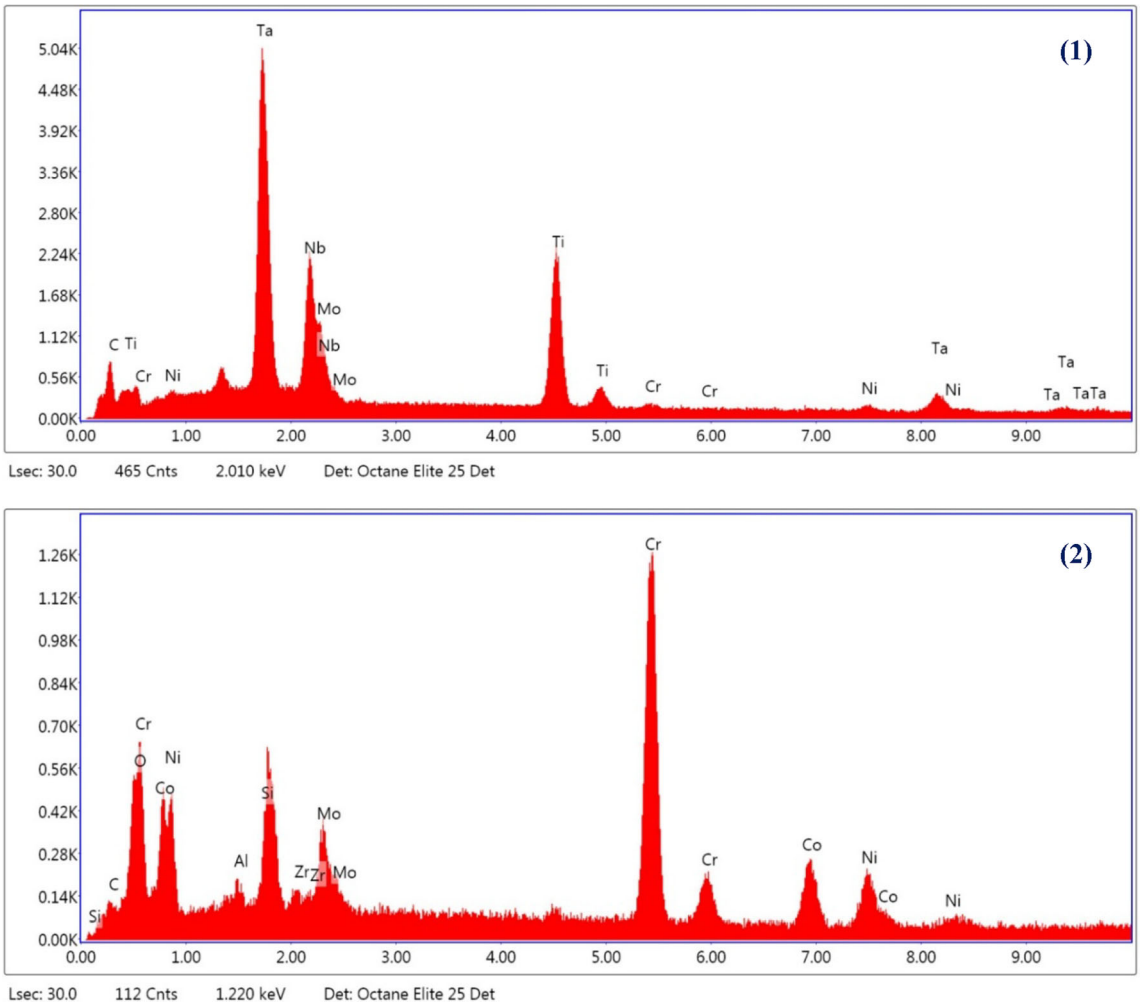

Fig. 17 EDS spectra, (1) of MC-carbide particles, (2) of $M_{23}C_6$ carbides

the VPS coating rich in NiCo elements shows the formation of $(Al, Cr)_2O_3$ oxides layer at the outer surface. This internal oxidation and continuous diffusion of O_2 into the interior quickly depletes the VPS coating of its available Al, Cr content. The presence of (Mo, Ti)-rich carbide particles in grains interior and $M_{23}C_6$ lines in the grain boundaries of the GTD-111 substrate was identified using the EDS spectra 2, and 3 of Fig. 5. Furthermore, the line profiles taken on VPS/GTD-111 strata as described in Fig. 6, confirm the diffusion and high concentration of (Cr, Al) elements at the outer surface of the VPS coating. This is due to the continuous formation of $(Cr, Al)_2O_3$ oxide scales during operation at 820 °C. Small oxide traces of Ti, Mo, Fe, and Co have been generated at the external surface of the VPS coating. A high concentration in Ni, and Co elements was detected in the non-affected coating zone and base substrate.

According to Fig. 7a, the microstructure and morphology of VPS/GTD-111 strata at the leading-edge region exhibit a less degradation extent in comparison with the trailing edge. In-depth examination of the corroded/oxidized leading-edge zone (pointed out by the white circle in Fig. 1) shows the formation of blocky Al_2O_3 oxide particles as shown in Fig. 7b. These Al_2O_3 oxide particles were the result of the O_2 diffusion into the GTD-111 substrate after the stripping off the VPS coating during operation. Figure 8 indicates the stability in elements concentration at the leading-edge strata. This steady state in the Ni, Co, Al, Cr, Fe, Ti, and Si concentrations is a sign of less degradation of leading-edge in comparison to the white circle region mentioned in Fig. 1. Figure 9a shows the presence of triangular γ' particles in the microstructure of the non-affected shank. In contrast, the γ' particles within blade leading-edge and trailing-edge take a spherical form as shown in Fig. 9b and c. From Table 2, it is clear that the initial γ' particles of 0.40 µm with a 39.8% volume fraction at the shank had grown up to 0.72 µm (45.48% volume fraction), and 0.98 µm (47% volume fraction) in the degraded leading-edge and trailing-edge, respectively. Based on expression (1), the degradation level of GTD-111

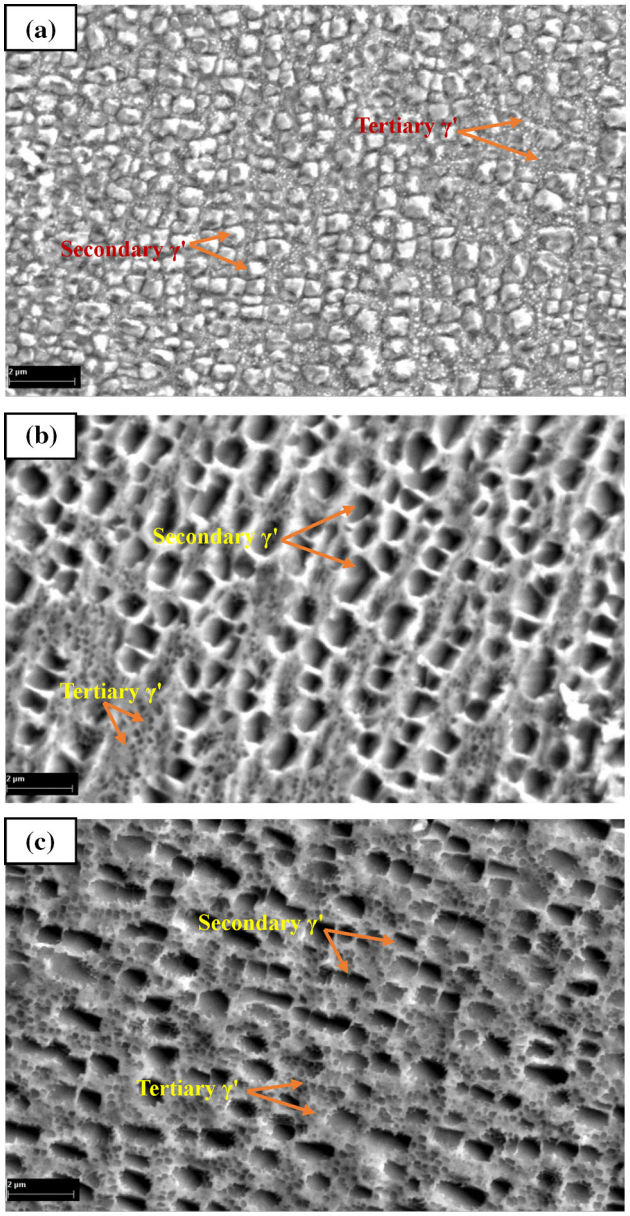

Fig. 18 SEM micrographs showing the $\gamma + \gamma'$ microstructure in the different IN738LC blade regions. (**a**) The shank. (**b**) The leading edge. (**c**) The trailing edge

substrate (D_i = 1, 1.8, up to 2.45) summarized in Table 2 is closely related to the γ' precipitates coarsening. From Table 3, hardness values are in good agreement with the values of the degradation index. This increase in hardness values from 420 (Hv) at the non-affected shank area up to 467 and 491 (Hv) in the leading-edge and trailing-edge corroded regions, respectively, is attributed to coarsening of the γ' precipitates and formation of the $M_{23}C_6$-lines network at grain boundaries.

Evaluation of the NiPtAl/IN738LC Strata

From the SEM micrograph of Fig. 10a, oxidation/corrosion of β-NiPtAl coating had provoked elements interdiffusion between the underlying IN738LC and the NiPtAl coating. The interdiffusion zone (IDZ) contain an elongated phase rich in (Ni, Co) Cr together with (Ti, Ta) Nb and (W, Ta) carbide particles. In addition, a needle σ phase was precipitated in the $\gamma + \gamma'$ microstructure beneath interdiffusion zone. It is known that this needle σ phase generated during operation have an impact on the creep resistance of the IN738LC blade [36]. The Al_2O_3 oxide scales are the result of the β-coating reaction with the exhausted hot gases. The precipitated $M_{23}C_6$-lines result from the degeneration of the irregular blocky MC-carbides within the γ-matrix of the IN738LC substrate. These $M_{23}C_6$-lines are rich in (Al, Cr, Ni, and Ti), while the isolated MC-carbides are rich in (Ta, Ti, and Nb). The local change in the composition of β-phase at the corroded/oxidized trailing-edge (Fig. 10b) is thought to be a consequence of aluminum loss, by diffusion in two directions toward the substrate and the outer surface of the coating. Oxidation in the β-layer reduces the amount of aluminum, which becomes lower and lower due the interdiffusion. The original β-phase had been transforming into a biphasic $\gamma' + \beta$ then to a $\gamma + \gamma'$ structure until attaining a lamellar structure. At this point, it becomes necessary to carry out blade refurbishment. Both inward diffusion of Al, Pt and outward diffusion of Co, Cr, Ti elements from IN738LC superalloy contributed to the transformation and consumption of the NiPtAl coating. EDS spectra (Fig. 11) obtained for areas marked 1, 2 and 3 in Fig. 10b, confirmed the nucleation of (Cr, Co) rich elongated nodules at the interdiffusion zone, and precipitation of needle (Ni, Co)Cr-W phase mixed with blocky (Ti, Ta)Nb carbides beneath the interdiffusion zone. Another important feature that occurred in Zr doped NiPtAl layer at the blade platform is the presence of thermal fatigue cracks due to the low strength and near full consumption of the coating, as shown in Fig. 12a. A multitude of C_3Al_4 precipitates were generated at the interdiffusion zone. The tortuous grain boundaries presented in Fig. 12b makes the blade more resistant to deformation. As shown in Fig. 14a, the continuous pitting corrosion and erosion attacks within the blade-cooling channel provoked the stripping of NiPtAl layer. The variety of micro-voids and C_3Al_4 particles generated in the β-layer (Fig. 14b) are also thought to be due to oxidation/corrosion attacks. The EDS spectrum in Fig. 15 indicate the formation of many $(Al, Cr)_2 O_3$, Fe_2O_3 oxide scales. A needle σ phase rich in (Ni, Co)Cr-W was precipitated beneath the interdiffusion zone. In addition, the (Ti, Ta)Nb particles found within the unaffected shank microstructure as shown in Fig. 16a, are identified using

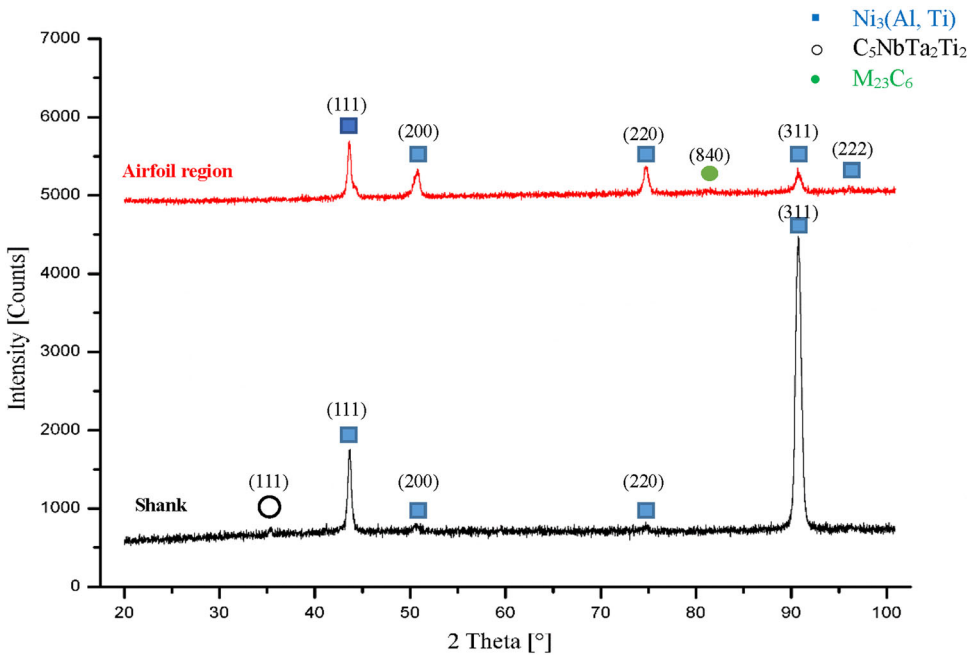

Fig. 19 X-ray diffraction (XRD) patterns of the non-affected shank and the degraded airfoil region

the EDS spectrum (1) of Fig. 17. These particles had degenerated during operation at ~ 800 °C according to the following reaction (Ti, Ta) $Nb + \gamma \rightarrow M_{23}C_6 + \gamma'$. The precipitation of $M_{23}C_6$ carbides at the grain boundaries of IN738LC substrate displayed in Fig. 16b is identified by EDS spectrum (2) of Fig. 17. The blade shank was found to consist of an austenitic γ matrix strengthened by two kinds of FCC γ'-(Ni_3, Al) precipitates (Fig. 18a): 0.52 µm secondary γ' precipitates with 34.22% volume fraction, and 0.1 µm tertiary γ' precipitates. These particles act as obstacles during operation against dislocation movement within superalloy $\gamma + \gamma'$ microstructure. The key phenomenon occurring in IN738LC blades is the secondary oval γ' particles growth from 0.84 µm with 37.47% volume fraction at the leading-edge to 1.11 µm with 39.71% volume fraction at the trailing-edge. From Fig. 18b and c, the mean size of tertiary γ' particles in the airfoil region estimated at 0.2 µm. The degradation (D_i) values mentioned in Table 2 show a good agreement between the γ' mean size and the IN738LC blade degradation level. Based on the increase in hardness (Table 3) from 430 (Hv) at the shank up to 619 (Hv) at the airfoil section is attributed to the formation of needle σ phase beneath the interdiffusion zone, the coarsening of γ' precipitates, and the $M_{23}C_6$ lines network formation at the grain boundaries. The growth (from 20.45 to 39.45 nm) and the orientation changes of γ' crystallites, as shown in Fig. 19 justify the degradation in hardness properties of the IN738LC blade.

Conclusions

Based on the metallurgical analysis of the degraded turbine blades, the following outcomes are outlined:

- Examination of the NiPtAl/IN738LC strata, after long-term thermal exposure shows the presence of elongated Cr, Co-rich nodules within the interdiffusion zone, and fragile σ-phase rich in (Ni, Co) Cr-W within the IN738LC substrate. This transformation to mixed $\gamma + \gamma' + \sigma$ morphology may have serious consequences on IN738LC blade hardness.
- Initiated cracks in the NiPtAl coating can propagates by thermal fatigue into the IN738LC substrate. Therefore, the NiPtAl coating could be changed to an overlay coating that has a good resistance to cracking.
- The VPS coating found on GTD-111 blade demonstrating superior hot corrosion resistance compared to the NiPtAl coating.
- The GTD-111 blade demonstrates superior hardness properties in comparison with IN738LC blade. This is attributed to the absence of the needle-like σ phase, and the slow growing of γ'-Ni_3 (Al, Ti) precipitates within GTD-111 substrate.

Acknowledgments The authors would like to thank the General Directorate of Scientific Research and Technological Development (DGRSDT, Algeria) in acknowledgment of their support to the present work (PRFU No. A11N01UN35012018004) and express their gratitude to the Dr. Med. A. Djeridane for his precious contribution.

References

1. N.N. Kazantseva, N.V. Natalia, N. Stepanova, M.B. Rigmant, *Superalloys: Analysis and Control of Failure Process* (CRC Press, Boca Raton, 2018)
2. R. Viswanathan, *Damage Mechanisms and Life Assessment of High Temperature Components* (ASM International, Cleveland, 1989)
3. R.C. Roger, *The Superalloys: Fundamentals and Applications* (Cambridge University Press, Cambridge, 2006)
4. S. Bose, *High Temperature Coatings* (Butterworth-Heinemann, Oxford, 2007)
5. M.P. Boyce, *Gas Turbine Engineering Handbook*, 4th edn. (Butterworth-Heinemann, Oxford, 2012)
6. C. Soares, *Gas Turbines: A Handbook of Air, Land and Sea Applications*, 2nd edn. (Butterworth-Heinemann, Oxford, 2014)
7. M.P. Boyce, *Gas Turbine Engineering Handbook*, 3rd edn. (Gulf Professional Publishing, Houston, 2006)
8. P. Walsh, P. Fletcher, *Gas Turbine Performance*, 2nd edn. (Blackwell Science, Hoboken, 2004)
9. D.K. Das, Microstructure and high temperature oxidation behavior of Pt-modified aluminide bond coats on Ni-base superalloys. Prog. Mater Sci. **58**, 151–182 (2013)
10. R. Darolia, Development of strong, oxidation and corrosion resistant nickel-based superalloys: critical review of challenges, progress and prospects. Int. Mater. Rev. **64**(6), 355–380 (2019)
11. M.P. Bacos, J.M. Dorvaux, O. Lavigne, R. Mévrel, M. Poulain, C. Rio, M.H. Vidal-Setif, Performance and degradation mechanisms of thermal barrier coatings for turbine blades: a review of Onera activities. AerospaceLab (3) (2011)
12. Z. Mazur, A. Luna-Ramírez, J.A. Juárez-Islas, Metallurgical assessment of degradation of a gas turbine bucket made of Inconel 738LC alloy after 24000 h in service, in *ASME Power Conference, Maryland* (2004), pp. 325–331
13. G.M. Shejale, D. Ross, Failure investigation of 1st stage buckets from frame 3002, 10 MW gas turbine unit, in *ASME Turbo Expo Conference, Vancouver, Canada* (2011), pp. 189–198
14. H. Rafiee, S. Rastegari, H. Arabi, Formation mechanism of IDZ during coating of IN738 by single step gas phase aluminizing. Can. Metall. Q. **50**(1), 85–90 (2011)
15. N. El-Bagoury, Q. Mohsen, Gamma prime and TCP phases and mechanical properties of thermally exposed nickel-base superalloy. Phase Trans. **84**(11-12), 1108–1122 (2011)
16. A.S. Golezani, M. Bageri, R. Samadi, Microstructural change and impact toughness property of Inconel 738LC after 12 years of service. Eng. Fail. Anal. **59**, 624–629 (2016)
17. K. Zhao, Y.H. Ma, L.H. Lou, Z.Q. Hu, Microstructure evolution of conventionally cast nickel base superalloy. Mater. Sci. Technol. **24**(10), 1245 (2008)
18. H.M. Tawancy, L.M. Al-Hadhrami, Comparative performance of turbine blades used in power generation: damage vs. microstructure and superalloy composition selected for the application. Eng. Fail. Anal. **46**, 76–91 (2014)
19. W.M. Miglietti, R. Curtis, J. Helm, Rejuvenation heat treatment and their role in the repair of IN738LC turbine components, in *ASME Turbo Expo Conference, Amsterdam, Netherlands*, GT-2002-30536
20. E. Lvova, A comparison of aging kinetics of new and rejuvenated conventionally cast GTD-111 gas turbine blades. J. Mater. Eng. Perform. **16**(2), 254–264 (2007)
21. E. Lvova, D. Norsworthy, Influence of service-induced microstructural changes on the aging kinetics of rejuvenated Ni-based superalloy gas turbine blades. J. Mater. Eng. Perform. **10**(3), 299–312 (2001)
22. V.S.K.G. Kelekanjeri, S.K. Sondhi, T. Vishwanath, F. Mastromatteo, B. Dasan, Coarsening kinetics of the bimodal γ' distribution in DS GTD111TM superalloy. WIT Trans. Eng. Sci. **72**, 251–262 (2011)
23. F.M. Shuaeib, K.Y. Benyounis, M.S.J. Hashmi, Material behavior and performance in environments of extreme pressure and temperatures, reference module in Mater. Sci. Mater. Eng. (2017)
24. I.M. Lifshitz, V.V. Slyozov, The kinetics of precipitation from supersaturated solid solutions. J. Phys. Chem. Sol. **19**, 35–50 (1961)
25. F. Mastromatteo, F. Niccolai, M. Giannozzi, U. Bardi, The coarsening kinetic of γ' particles in nickel-based superalloys during aging at high temperatures, in *ASME Turbo Expo Conference, Vienna, Austria*, GT2004-54214
26. A. Dadkhah, A. Kermanpur, on the precipitation hardening of the directionally solidified GTD-111 Ni-base superalloy: microstructures and mechanical properties. Mater. Sci. Eng. A **685**, 79–86 (2017)
27. G. Lvov, V.I. Levit, M.J. Kaufman, Mechanism of primary MC carbide decomposition in Ni-base superalloys. Metall. Mater. Trans. A **35**(6), 1669–1679 (2004)
28. R. Boestaman, V.P. Swaminathan, H.L. Bernstein, Protective coatings and degradation experiences for first stage buckets on GE MS-5002B/C gas turbines, in *ASME Turbo Asia Conference, Jakarta, Indonesia, TA* (1996)-32
29. Palo Alto, Blade Life Management: Coating Systems, EPRI, CA, TR (1999)-113899
30. R. Sushila, A.K. Agrawal, V. Rastogi, Failure analysis of a first stage IN738 gas turbine blade tip cracking in a thermal power plant. Eng. Fail. Anal. **8**, 1–10 (2017)
31. V.D. Divya, U. Ramamurty, A. Paul, Effect of Pt on interdiffusion and mechanical properties of the γ and γ' phases in the Ni–Pt–Al system. Philos. Mag. **92**(17), 2187–2214 (2012)
32. R. Bauer, K. Schneider, H.W. Grünling, Experience with platinum aluminide coatings in land-based gas turbines. High Temp. Technol. **3**(2), 59–64 (1985)
33. P. Caron, O. Lavigne, Recent Studies at Onera on Superalloys for Single Crystal Turbine Blades, AerospaceLab, (3), (2011)
34. W.S. Walston, J.C. Schaeffer, W.H. Murphy, A new type of microstructural instability in superalloys-SRZ, Superalloys, TMS, Warrendale, PA (1996), pp. 9–18
35. T. Narita, Diffusion barrier coating system concept for high temperature applications. Can. Metal. Q. **50**, 3 (2011). https://doi.org/10.1179/1879139511y.0000000014
36. I. Calliari, M. Dabala, A. Zambon, Microstructural characterization of a Pt-aluminide coated IN738LC. J. Mater. Eng. Perform. **10**(3), 258–262 (2001)